IOP Publishing Superconductor Science and Technology
Supercond. Sci. Technol. 33 (2020) 055006 (6pp) https://doi.org/10.1088/1361-6668/ab7c7c

Residual oxygen responsible for universal superconducting phase diagram in annealed $FeSe_{1-x}Te_x$

David M Uhrig[1,2,3], Grant V M Williams[2,3], Gabriel Bioletti[1,2,3] and Shen V Chong[1,3]

[1] Robinson Research Institute, Victoria University of Wellington, Lower Hutt 5010, New Zealand
[2] School of Chemical and Physical Sciences, Victoria University of Wellington, Wellington 6140, New Zealand
[3] MacDiarmid Institute for Advanced Materials and Nanotechnology, Victoria University of Wellington, Wellington 6140, New Zealand

E-mail: david.uhrig@vuw.ac.nz

Received 3 December 2019, revised 11 February 2020
Accepted for publication 4 March 2020
Published 24 March 2020

Abstract

We report the results from a comprehensive study of the effect that annealing $FeSe_{0.35}Te_{0.65}$ single crystals in different atmospheres has on the surface chemistry, the superconducting transition temperature, T_c, and the critical current density, J_c. A review of the literature and our data shows that annealing in oxygen, nitrogen, air or vacuum atmosphere leads to a universal superconducting phase diagram that is independent of the variance in the as-grown properties. We show that atmospheres with an oxygen partial pressure of $p > 10^{-3}$ hPa during annealing are necessary to improve the superconducting properties in this compound. This is demonstrated by Raman and magnetisation measurements on air, nitrogen, or low vacuum annealed $FeSe_{0.35}Te_{0.65}$ samples, which show that the improvement in the superconducting properties is strongly correlated to the formation of a thin iron oxide surface layer. However, annealing under high vacuum does not lead to the formation of an iron oxide layer and no improvement in the superconducting properties is observed. Our findings show that the previously reported improvements in the superconducting properties after annealing under vacuum or in nitrogen are thus likely to have been caused by residual oxygen. Furthermore, we propose a diffusion model for the formation of the iron oxide layer as the driving force for the reduction of interstitial excess iron that suppresses superconductivity in this compound. Overall, our results show that the presence of an iron reactant, such as oxygen, during annealing is necessary to improve the superconducting properties of $FeSe_{1-x}Te_x$.

Keywords: iron chalcogenide, iron-based superconductors, FeSeTe, Raman spectroscopy, iron oxide, annealing, residual oxygen

(Some figures may appear in colour only in the online journal)

1. Introduction

The tellurium doped iron selenide family ($FeSe_{1-x}Te_x$) of superconductors has attracted much attention due to its simple crystal structure compared to other iron-based superconductors and the highly tuneable superconducting transition temperature, T_c, by ionic liquid gating [1], under hydrostatic pressure [2], and the drastic increase of T_c for monolayer FeSe [3]. However, previous reports of as-grown single crystals show a significant variance in many fundamental properties, such as the doping-dependent superconducting phase diagram and the critical current density, J_c [4–7]. This variance is likely to be related to differences in the amount of interstitial excess iron, which is invariably present in as-grown $FeSe_{1-x}Te_x$ single crystals and has been shown to suppress superconductivity in this family of superconductors [8–12].

Consequently, the reported properties in the literature have been determined by the amount of interstitial excess iron rather than the intrinsic properties of this compound. To probe the intrinsic properties of this compound, it is therefore essential to establish growth and post-processing procedures that guarantee reproducible high-quality samples with low amounts of interstitial excess iron. Thus far, annealing in oxygen containing atmospheres has been shown to reduce the amount of interstitial excess iron within the sample [13] via the formation of iron oxides on the surface of the sample [14–16] and consequently improving the superconducting properties. However, improvements in the superconducting properties have also been reported for annealing in various other atmospheres such as nitrogen [4] or under vacuum [7]. This is surprising because neither pure nitrogen [17, 18] nor vacuum annealing should lead to binary compounds under typical annealing conditions. Hence, it remains unclear if the observed improvement in the superconducting properties in this scenario is also driven by a reduction in the amount of interstitial excess iron and, if so, what process would be driving it. Therefore, further research is required to advance our understanding of the underlying physics of the annealing process and to unequivocally identify the processes leading to the improvement of the superconducting properties in this compound [16, 19–21].

In this paper, we present the results from a study of the effect of annealing in different atmospheres on the surface chemistry and superconducting properties of $FeSe_{0.35}Te_{0.65}$ single crystal. Unlike previous reports, we do not only focus on the change in T_c and J_c, but also relate them to changes in the structure and the chemical composition. Specifically, we used Raman spectroscopy to identify the formation of different iron oxides after annealing that are hard to identify using other commonly employed techniques such as energy dispersive x-ray spectroscopy [4, 12, 15] or electron energy loss spectroscopy [14]. We show that annealing in air, nitrogen, and low vacuum conditions leads to the formation of a thin iron oxide surface layer. Annealing under high vacuum, however, only leads to the formation of minute amounts of magnetite (Fe_3O_4). We attribute the appearance of an iron oxide surface layer to an oxygen-induced reduction in the interstitial excess iron that is linked with increases in T_c and J_c that are only observed when the oxygen partial pressure is greater than 10^{-3} hPa. We propose a diffusion model that describes the reduction of interstitial excess iron during annealing driven by the reaction of the iron close to the surface with a reactant provided by the annealing atmosphere. We show that our results and analyses strongly point to the reduction of interstitial excess iron via the reaction with an annealing agent at the surface as the driving factor for improved superconducting properties.

2. Experimental methods

$FeSe_{1-x}Te_x$ single crystals were synthesised using the self-flux method (for details of the synthesis conditions see ref. [16]). As-grown samples with a typical size of $1000 \times 1000 \times 100\ \mu m^3$ were annealed for 2 h at 300 °C in air, nitrogen or under low or high vacuum. For air annealing, the furnace tube was continuously flushed with dry air at a rate of 80 $cm^3\ min^{-1}$. For the nitrogen annealing, the furnace tube was carefully purged by first baking it at 600 °C and then nitrogen flushing and pumping it down to a high vacuum ($p \approx 10^{-5}$ hPa) several times to reduce the amount of residual air and moisture. The furnace tube was then either sealed at constant pressure or continuously flushed with 99.998% ($O_2 < 5$ ppm) purity nitrogen. For vacuum annealing, the furnace tube was again baked at 600 °C to reduce the amount of residual moisture and then continuously pumped using just a rotary vane pump (low vacuum, $p \approx 10^{-2}$ hPa) or combined with a turbo molecular pump (high vacuum, $p \approx 10^{-5}$ hPa). Raman analysis of the samples was performed using a confocal Raman microscope with a laser wavelength of 633 nm. Magnetisation measurements were carried out using a vibrating sample magnetometer (VSM) in a *Quantum Design* Physical Property Measurement System. For the zero-field-cooled (ZFC), field-cooled (FC) magnetisation, and magnetic hysteresis loop measurements, the temperature or magnetic field were stabilised at every set point.

3. Results and discussion

Figure 1(a) shows the critical temperature, T_c, of as-grown $FeSe_{1-x}Te_x$ samples from several reports [4–7] and our own work for different selenium concentrations. We find that T_c of the as-grown samples with similar Se concentration varies greatly between different reports. In fact, not only is there a wide variation between different reports, but as in the case of Noji *et al* [7], even individual studies report a wide range of critical temperatures for samples with the same selenium concentration. Figure 1(b) shows the corresponding T_c of the same reports and our work after annealing in different atmospheres or in a vacuum. Interestingly, besides the commonly reported increase of T_c after annealing [4–7, 12], our summary shows that annealing leads to a universal superconducting phase diagram that is independent of the properties of the as-grown samples.

The absence of a universal superconducting phase diagram for as-grown $FeSe_{1-x}Te_x$ from our study and four other studies (see figure 1(a)) is due to different amounts of interstitial excess iron that arises from variations in the synthesis conditions. Excess iron is known to supress T_c [8–12], and hence variations in the excess iron fraction leads to the observed differences in T_c. The universal superconducting phase diagram that appears after annealing from all six studies (figure 1(b)) is likely to be due to a reduction in the excess iron fraction to a common value. Thus, our comparison of reports from the literature with our data vividly illustrates that annealing is crucial to obtain reproducible high-quality samples, as was also previously pointed out by other authors [14, 20–22].

Even though the beneficial effect of annealing has been widely studied [4–7, 12, 22], the underlying physics of the

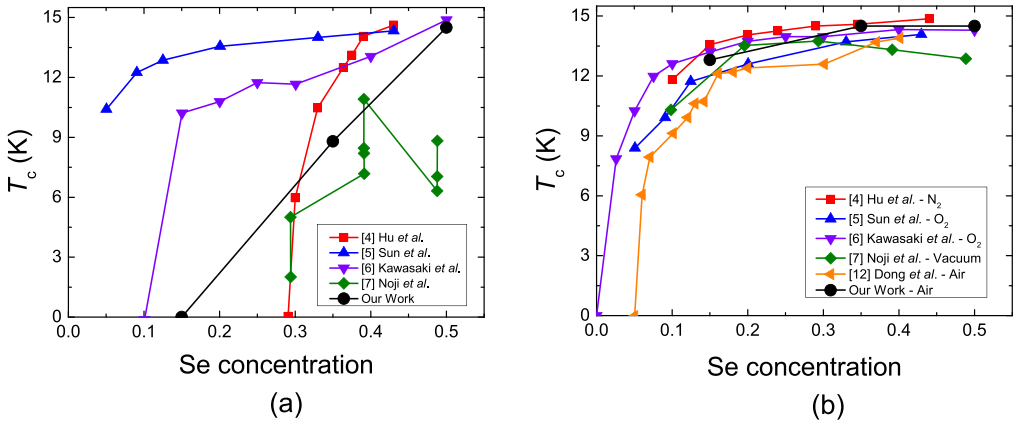

Figure 1. (a) Plot of T_c versus the Se concentration for as-grown $FeSe_{1-x}Te_x$ from the literature [4–7] and our own work (filled circles). (b) Plot of T_c versus the Se concentration of $FeSe_{1-x}Te_x$ from the literature [4–7, 12] and our own work (filled circles) after annealing in different atmospheres.

process that leads to this improvement in the superconducting properties is still not fully understood. Moreover, figure 1(b) might suggest that annealing in different atmospheres has a similar effect on T_c, but there is still substantial disagreement in the literature over the beneficial effects of annealing in different atmospheres [5, 6]. For example, annealing under vacuum or nitrogen have both been found to have a beneficial effect [4, 7] as well as no effect at all [23]. To help clarify the situation, we used Raman spectroscopy to investigate the effect of annealing in air, nitrogen, under low and high vacuum on the surface chemistry. The changes in the surface chemistry were then correlated to changes in the magnetic susceptibility, and the critical superconducting current density, J_c, estimated from hysteresis loop measurements using the Bean model [24, 25].

Figure 2(a) shows the Raman spectra after annealing six samples in air. As previously reported [16], we find that annealing in air leads to the formation of magnetite (Fe_3O_4) and hematite (α-Fe_2O_3) on the surface of the sample. The bulk within the sample remains iron oxide free [16]. This shows that oxygen does not diffuse into the sample and that the formation of iron oxide is limited to the surface. Figure 2(b) is a plot of the Raman spectra of three samples after annealing in nitrogen (<5 ppm oxygen). Iron oxide is again evident in the Raman spectra but in this case purely magnetite, which is a less oxidised form of iron than hematite. The appearance of iron oxide on the surface of the samples is surprising. It indicates that even a low oxygen fraction (<5 ppm) is enough to partially oxidise iron. The Raman spectra of low and high vacuum annealed samples are shown in figure 2(c). In the case of annealing under high vacuum conditions, the Raman spectrum is almost unchanged after annealing except for a very small peak from a magnetite Raman mode at 667 cm^{-1}. One of the samples (figure 2(c), orange curve) was annealed for 24 h to demonstrate that even prolonged annealing does not lead to the formation of iron oxide when annealing in high vacuum conditions. After 24 h of high vacuum annealing, and subsequent characterisation, the same sample was annealed under low vacuum conditions ($p \approx 10^{-2}$ hPa) for 2 h. In contrast to high vacuum annealing, we find that two hours of low vacuum annealing is enough to form an iron oxide surface layer of magnetite, similar to that observed for nitrogen annealing. Thus, there is still enough residual oxygen present for the formation of iron oxide under low vacuum. It is only under high vacuum conditions that the amount of residual oxygen is reduced enough to prevent the formation of a thick iron oxide surface layer.

Figures 2(d)–(f) show the ZFC and FC magnetic susceptibility after annealing. Each susceptibility curve was corrected to account for demagnetisation effects [26]. For ease of comparison, the susceptibility and Raman data for each sample are represented using the same colour within the respective annealing conditions. Figure 2(d) shows the susceptibility for the samples before (dashed lines) and after (full lines) air annealing. The as-grown samples show a significant variance in T_c, the superconducting transition width, and only partial diamagnetic shielding at the lowest temperature. After annealing, all samples show a superconducting transition around 14 K with a relatively similar transition width and perfect diamagnetic shielding at low temperatures ($\chi(2\text{K}) = -1$). Interestingly, we find that nitrogen annealing (see figure 2(e)) also leads to an increase in T_c, a reduction in the transition width, and perfect diamagnetic shielding very similar to what we observed for the air-annealed samples. When taking into consideration the Raman analysis shown in figures 2(a) and (b), it is likely that the observed increase in T_c, and the similarity with the air-annealed samples is due to the residual oxygen in the N_2 gas (<5 ppm) rather than being due to nitrogen. The residual oxygen led to the formation of iron oxide and therefore a reduction in the amount of interstitial excess iron and the related increase in T_c. In the case of high vacuum annealing (figure 2(f)), we find little effect on the critical temperature, the temperature dependence of the ZFC susceptibility and the diamagnetic shielding at the lowest temperature. This observation is consistent with the Raman analysis above that showed only a very small amount of iron oxide was formed and, hence, minimal reduction in interstitial excess iron. After annealing the same sample under low vacuum conditions, we again observe an increase in T_c, which is driven by the residual oxygen present in low vacuum.

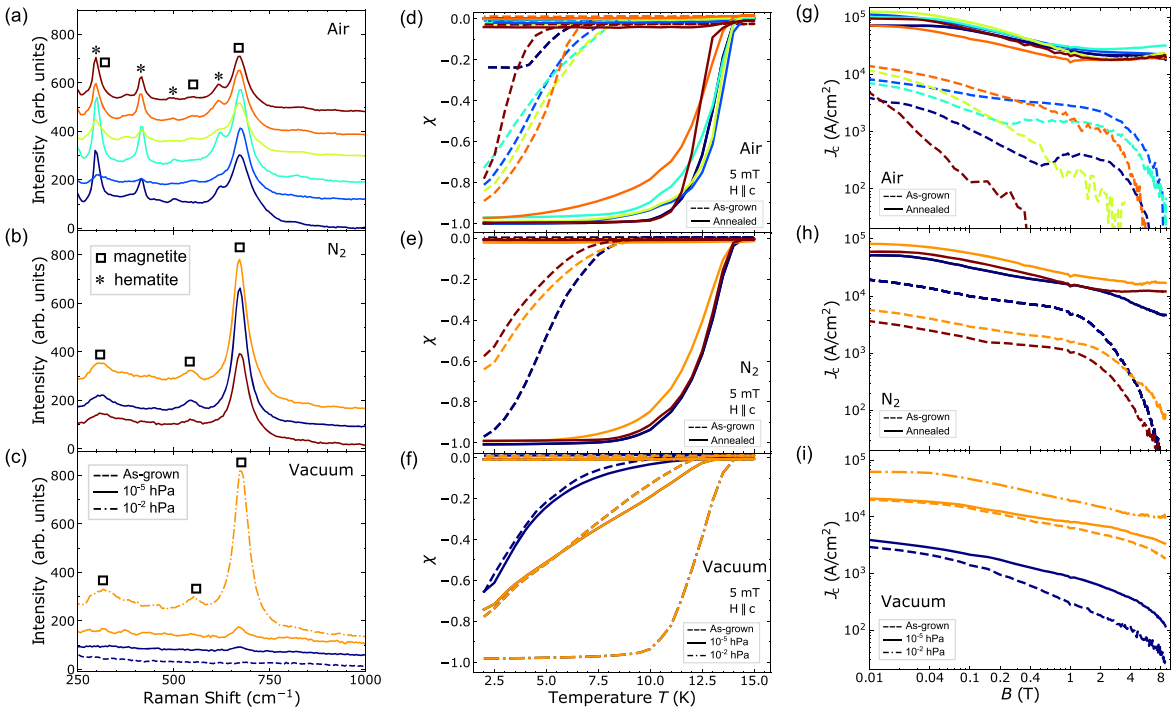

Figure 2. (Left) Raman spectra of several $FeSe_{0.35}Te_{0.65}$ samples after annealing in (a) air, (b) nitrogen, and (c) under vacuum. For ease of comparison, the spectra have been shifted on the vertical axis. (Center) Plot of the demagnetisation-corrected ZFC and FC magnetic susceptibility of several as-grown (dashed line) $FeSe_{0.35}Te_{0.65}$ single crystals and after annealing (full line) in (d) air, (e) nitrogen, and under (f) vacuum. (Right) Plot of J_c at 2.2 K for several as-grown $FeSe_{0.35}Te_{0.65}$ single crystals (dashed line) and after annealing (full line) in (g) air, (h) nitrogen, and (i) under vacuum. The Raman, magnetic susceptibility, and J_c data for each sample are represented by the same colour for each respective annealing condition.

The effect of annealing in different environments on J_c can be seen in figures 2(g)–(i). It is apparent that annealing in air, nitrogen, or low vacuum resulted in a large increase in J_c for all the samples. Only the high vacuum annealed samples show little change in J_c after annealing. Therefore, the formation of the iron oxide layer and the resulting reduction of interstitial excess iron is the driving factor for the observed increase in J_c.

Our analysis of air, nitrogen, low- and high-vacuum annealed samples indicates that the improvement in the superconducting properties is directly related to the formation of a thin iron oxide layer, which reduced the amount of interstitial excess iron within the samples and thereby improved the superconducting properties. It is extremely difficult to measure the actual iron oxide thickness after annealing in different atmospheres. However, a very simple calculation of the iron oxide thickness can be used to illustrate the effect of annealing in different oxygen partial pressures. This was done assuming the ideal gas law, a fixed sealed gas volume, and that all the available oxygen reacts with Fe to form Fe_3O_4 on the surface of the sample. The different atmospheres are nitrogen (99.998% pure nitrogen with oxygen <5 ppm), low vacuum ($p_{\mathrm{vac,\,low}} = 10^{-2}$ hPa), and high vacuum ($p_{\mathrm{vac,high}} = 10^{-5}$ hPa). The tube furnace volume was 0.741 and the typical sample dimension was $1 \times 1 \times 0.1$ mm^3. Under these assumptions the estimated Fe_3O_4 film thicknesses are, 840 nm (3.0% excess Fe reduction) for nitrogen, 350 nm (1.2% excess Fe reduction) for low vacuum, and 0.35 nm (0.001% excess Fe reduction) for high vacuum. This simple calculation shows that nitrogen and low vacuum annealing is sufficient to remove interstitial excess iron by greater than 1% while high vacuum annealing has negligible effect, which is consistent with the observed oxygen-induced changes in the superconducting properties.

Based on these results, we propose a model where the removal of the interstitial excess iron is driven by a diffusion process of the interstitial excess iron caused by a reaction with oxygen at the surface and a resulting iron concentration gradient. The general idea of this proposed process is depicted at different characteristic times in figure 3 for the case of annealing in an oxygen-containing atmosphere. The figures show three two-dimensional $FeSe_{1-x}Te_x$ layers with gaps in the layer to symbolise lattice defects such as grain boundaries, cracks or twin-boundaries. The full circles represent the different atom sites for iron (brown), selenium and tellurium (blue), interstitial iron (red), and the oxygen in the annealing gas (green). The dashed red circles represent previously occupied interstitial sites. The grey background qualitatively illustrates the interstitial iron concentration from high to low as grey to white, respectively. At $t = t_0$, the sample is at room temperature in the initial as-grown state and a substantial amount of interstitial iron is distributed throughout the sample. When the temperature is increased ($t = t_1$), the interstitial excess iron close to the surface starts to react with oxygen to form iron oxides. This leads to a reduction in the iron concentration near the surface and results in an iron concentration

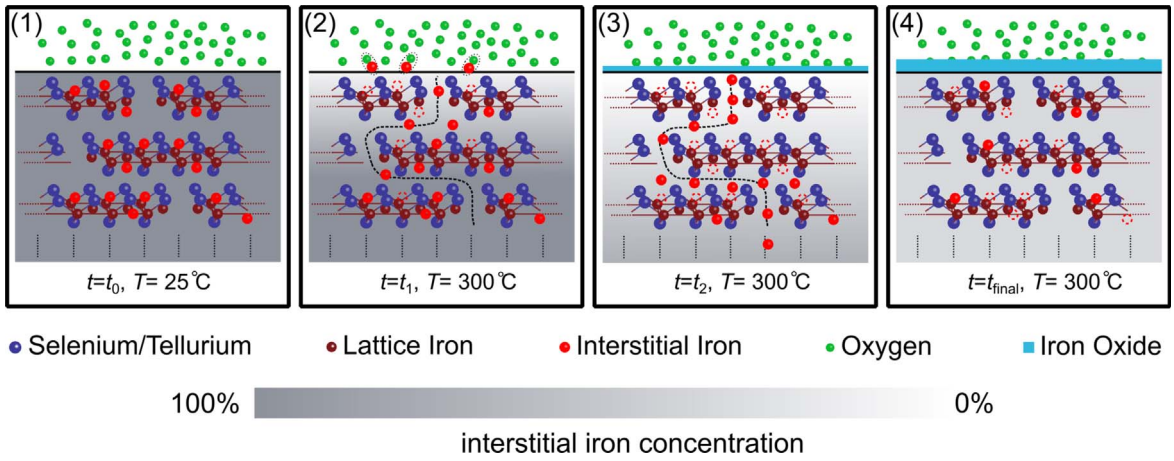

Figure 3. Schematic drawing of the proposed model for the diffusion of interstitial iron towards the surface. The schematics depict four characteristic stages at different times in the annealing process: (1) before annealing, (2) the start of the annealing process, (3) after some time has passed ($t_2 > t_1$) and lastly (4) after the annealing. The grey background symbolizes the interstitial excess iron concentration at the respective depth—the darker the grey, the higher the concentration and vice versa.

gradient that drives more interstitial excess iron from deeper in the sample towards the surface region. After holding at 300 °C for a time $t = t_2$, a thin FeO_x layer has started to grow on the sample surface. At $t = t_{final}$, the FeO_x layer has become thick enough to act as a diffusion barrier shielding the external oxygen from reacting with iron inside the sample. The remaining interstitial excess iron within the sample cannot react with the oxygen and the concentration gradient starts to decrease as the sample reaches a steady state. In this final state, the interstitial iron will again be uniformly distributed throughout the sample, but the total amount of interstitial iron within the sample is depleted due to the formation of the iron oxide on the surface.

In this scenario, there are two characteristic interstitial iron diffusion paths, in-plane diffusion and inter-plane diffusion. In-plane diffusion is very fast due to the two-dimensional layered structure of $FeSe_{1-x}Te_x$. Therefore, we propose the preferential inter-plane iron diffusion through defects, depicted by the dashed black line, that act as 'fast paths' [27]. Specifically, the iron atoms diffuse in-plane until they reach a defect that allows for fast inter-plane diffusion [27]. These preferential diffusion paths align with the formation of patterns on the surface as reported in our previous work [16]. Overall, the key requirement for our model is that the annealing atmosphere contains an element for the interstitial iron to react with during annealing. The iron reactant could be oxygen, as in our case, or other elements that form iron compounds. This is consistent with the observed formation of iron compounds and the related improvement in the superconducting properties when annealing in Te [28, 29], Se [30], S [30] or O [5] and based on our results also in the case of N_2 or low vacuum annealing due to residual oxygen.

4. Conclusions

In conclusion, we find a significant improvement in T_c and J_c in $FeSe_{1-x}Te_x$ after annealing in air, nitrogen, and low vacuum that can be attributed to the oxygen present during annealing that drives a reduction in the amount of interstitial excess iron within the sample. This conclusion is consistent with our results from annealing in high vacuum, where only negligible changes occurred. We propose a model where interstitial excess iron diffuses rapidly between the weakly van der Waals coupled $FeSe_{1-x}Te_x$ layers and then through lattice defects in the $FeSe_{1-x}Te_x$ layers (grain boundaries, cracks or twin-boundaries) to the surface resulting in a reduction of interstitial iron inside the sample. The process is driven by oxygen that reacts with the interstitial excess iron in the near surface region and forms an iron oxide layer. This creates an iron concentration gradient that drives more iron to the surface. Eventually the iron oxide layer is too thick for oxygen to diffuse through it and interstitial excess iron becomes uniformly distributed, but at a lower fraction. Our results clarify the origin of the uncertainty around annealing in different atmospheres and points at residual oxygen as the iron reactant responsible for decreasing the amount of interstitial excess iron. Using our data and other data from the literature, we find that a sufficient oxygen-induced reduction in the interstitial excess iron reveals a universal superconducting phase diagram. Our results can be extended to other studies that report annealing in atmospheres with different elements that also react with the interstitial excess iron.

Acknowledgments

We acknowledge funding by the Marsden Fund of New Zealand (VUW1608) and the MacDiarmid Institute for Advanced Materials and Nanotechnology.

ORCID iDs

David M Uhrig https://orcid.org/0000-0002-0644-8346
Gabriel Bioletti https://orcid.org/0000-0001-6317-3310

References

[1] Lei B *et al* 2016 *Phys. Rev. Lett.* **116** 077002
[2] Medvedev S *et al* 2009 *Nat. Mater.* **8** 630–3
[3] Ge J-F, Liu Z-L, Liu C, Gao C-L, Qian D, Xue Q-K, Liu Y and Jia J-F 2014 *Nat. Mater.* **14** 285–9
[4] Hu J, Wang G C, Qian B and Mao Z Q 2012 *Supercond. Sci. Technol.* **25** 084011
[5] Sun Y, Yamada T, Pyon S and Tamegai T 2016 *Sci. Rep.* **6** 32290
[6] Kawasaki Y, Deguchi K, Demura S, Watanabe T, Okazaki H, Ozaki T, Yamaguchi T, Takeya H and Takano Y 2012 *Solid State Commun.* **152** 1135–8
[7] Noji T, Suzuki T, Abe H, Adachi T, Kato M and Koike Y 2010 *J. Phys. Soc. Japan* **79** 085711
[8] McQueen T M *et al* 2009 *Phys. Rev.* B **79** 014522
[9] Zhang L, Singh D J and Du M H 2009 *Phys. Rev.* B **79** 012506
[10] Lei H, Hu R, Choi E S, Warren J B and Petrovic C 2010 *Phys. Rev.* B **81** 094518
[11] Liu T J *et al* 2009 *Phys. Rev.* B **80** 174509
[12] Dong C, Wang H, Li Z, Chen J, Yuan H Q and Fang M 2011 *Phys. Rev.* B **84** 224506
[13] Sun Y, Tsuchiya Y, Taen T, Yamada T, Pyon S, Sugimoto A, Ekino T, Shi Z and Tamegai T 2014 *Sci. Rep.* **4** 4585
[14] Hu H *et al* 2012 *Phys. Rev.* B **85** 064504
[15] Komiya S, Hanawa M, Tsukada I and Maeda A 2013 *J. Phys. Soc. Japan* **82** 064710
[16] Uhrig D M, Williams G V M, Bioletti G and Chong S V 2019 *Supercond. Sci. Technol.* **32** 074002
[17] Ertl G, Huber M and Thiele N 1979 *Z. Nat.forsch.* **34a** 30–9 (http://zfn.mpdl.mpg.de/data/Reihe_A/34/ZNA-1979-34a-0030.pdf)
[18] Metin E and Inal O T 1987 *J. Mater. Sci.* **22** 2783–8
[19] Zhou W, Sun Y, Zhang S, Zhuang J, Yuan F, Li X, Shi Z, Yamada T, Tsuchiya Y and Tamega T 2014 *J. Phys. Soc. Japan* **83** 064704
[20] Yamada T, Sun Y, Pyon S and Tamegai T 2016 *J. Phys. Soc. Japan* **85** 024712
[21] Lima M S L, ElMassalami M, Deguchi K, Takeya H and Takano Y 2018 *J. Phys.: Conf. Ser.* **969** 012056
[22] Sun Y, Shi Z and Tamegai T 2019 *Supercond. Sci. Technol.* **32** 103001
[23] Sun Y, Taen T, Tsuchiya Y, Shi Z X and Tamegai T 2013 *Supercond. Sci. Technol.* **26** 015015
[24] Bean C P 1962 *Phys. Rev. Lett.* **8** 250–3
[25] Bean C P 1964 *Rev. Mod. Phys.* **36** 31–9
[26] Prozorov R and Kogan V G 2018 *Phys. Rev. Appl.* **10** 014030
[27] Laughlin D and Hyono K 2014 *Physical Metallurgy* (Amsterdam: Elsevier)
[28] Tamegai T, Sun Y, Yamada T and Pyon S 2016 *IEEE Trans. Appl. Supercond.* **26** 7300205
[29] Sun Y, Tsuchiya, Yamada T, Taen T, Pyon S, Shi Z and Tamegai T 2013 *J. Phys. Soc. Japan* **82** 093705
[30] Sun Y, Tsuchiya Y, Yamada T, Taen T, Pyon S, Shi Z and Tamegai T 2013 *J. Phys. Soc. Japan* **82** 115002